

Electronic structure of stacking faults in hexagonal graphite

M. Taut, K. Koepernik, and M. Richter

IFW Dresden, PO Box 270116, D-01171 Dresden, Germany

(Dated: (September 13, 2021))

Abstract

We present results of self-consistent, full-potential electronic structure calculations for slabs of hexagonal graphite with stacking faults and for slabs with one displaced surface layer. There are two types of stacking faults, which differ qualitatively in their chemical bonding picture. We find, that both types induce localized interface bands near the symmetry line K-M in the Brillouin zone and a related peak in the local density of states (LDOS) very close to the Fermi energy, which should give rise to a dominating contribution of the interface bands to the local conductivity at the stacking faults. In contrast, a clean surface does not host any surface bands in the energy range of the π and σ bands, and the LDOS near the surface is even depleted. On the other hand, displacement of even one single surface layer induces a surface band near K-M. A special role play p_z -bonded dimers (directed perpendicular to the layers) in the vicinity of one type of stacking faults. They produce a half-filled pair of interface states / interface resonances. The formation energy of both types of stacking faults and the surface energy are estimated.

PACS numbers: 73.21.Ac, 73.22.Pr, 73.20.At, 81.05.U-

I. INTRODUCTION

Graphitic systems gained a renewed interest (after the intercalation, fullerene, and nanotube rushes) following the invention of techniques to produce thin two-dimensional systems in the form of thin slabs or even mono-layers (for recent review see e.g. Refs. 1–4). There is, however, another form of two-dimensionality, namely stacking faults in bulk hexagonal (AB) graphite with related interface states. These states are interesting, because they have been suspected to play a role in the observed integer quantum Hall effect [5, 6] in bulk graphite. As we will show, they may also contribute considerably to the electronic conductivity.

The electronic states in graphitic piles can be grouped into π and σ states. The π bands are mainly formed by p_z orbitals, they are responsible for the electronic structure around the Fermi energy ε_F . The σ bands with a total band width of about 40 eV are formed by the three $sp_{(2)}$ linear combinations of s , p_x , and p_y orbitals and lie more than 3 eV below and more than 8 eV above ε_F (see Fig. 1). It is mainly the σ bands which stabilize the honeycomb structure of the graphene layers, while the π bands account for their intriguing physical properties.

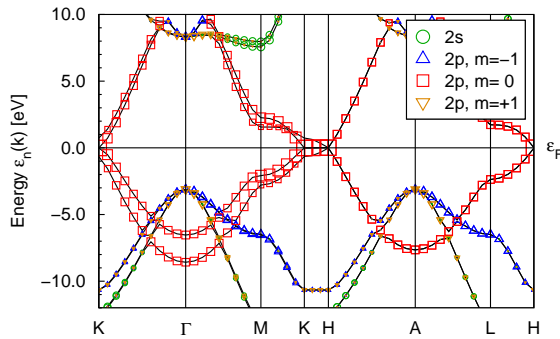


FIG. 1. (color online) Band weights of the orbitals of the second shell at a **single atom** in hexagonal bulk graphite. The figure for the **chain atoms** (not shown) differs mainly near the line K-H around the Fermi energy (see the zoom in Fig. 3).

The importance of the electronic structure of stacking faults in graphite results from their abundance in all kinds of samples and from the fact that they host localized interface bands [6, 7]. The large probability of their occurrence has its origin in the small energy difference between different stacking sequences, which for its part can be traced back to the large difference between intra-layer and inter-layer overlap integrals. The largest interlayer overlap integral between p_z orbitals, γ_1 , is ≈ 0.4 eV, and the largest intra-layer overlap integral between p_z orbitals, γ_0 , is ≈ 2.6 eV [8, 9]. The overlap integrals between $sp_{(2)}$ orbitals are not included in the common tight-bonding models. It follows from the large σ gap and bandwidth, that they are much larger than γ_0 .

Fig. 2 shows the three possible highly-symmetric relative locations of graphene layers

within a hexagonal unit cell. In constructing stacking faults, we consider slabs of AB-stacks (which would form hexagonal graphite, if the slab was infinite), followed by a C-layer, whereby the C-layer is already part of the subsequent CA- or CB-stack. In this way, two kinds of stacking faults are generated (see Sect. IV). Generally, we rule out the neighborhood of two identical layers, because of their large contribution to the total energy (see [10] and our results below). Such a slab with a stacking fault is either periodically repeated (without any surface), or surrounded by slabs of vacuum and then periodically repeated. In the latter case we can study interfaces and surfaces in the same calculation. In case of periodic repetition without vacuum we have the advantages that the unit cell can be chosen to have a higher symmetry than a slab, and that the large surface energy does not mask the small total energy differences between the two types of stacking faults. Therefore, total energies of stacking faults were calculated in the geometry without surfaces, but one-electron spectra and surface energies in slabs with surfaces. Additionally, we consider pure AB-slabs with surfaces (see Sect. III) and with a single displaced surface layer of type C on either side (see Sect. VI). The width of the vacuum layer was chosen to be 6 interlayer distances throughout this paper.

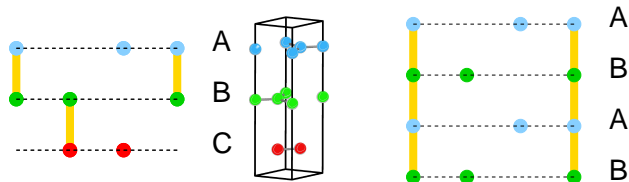


FIG. 2. (color online) The three basic layers A (blue), B (green), and C (red) in graphitic stacks within a hexagonal unit cell. Left: atoms on a plane in a hexagonal unit cell of rhombohedral (ABC) graphite, and right: in two unit cells of hexagonal (Bernal) stacking. Saturated p_z bonds are indicated by yellow perpendicular bars.

Two previous works on stacking faults [6, 7] considered two phenomenological overlap integrals (γ_0 and γ_1) within a mostly analytical model calculation. While this model correctly predicts the existence (not the details) of interface bands at one of the two possible stacking faults in hexagonal graphite, it cannot describe the band structure around ε_F of hexagonal (Bernal) or rhombohedral bulk graphite even qualitatively (see Ref. 7 and references therein). Former self-consistent slab calculations on graphitic slabs can be found in Refs. [11–15].

In this paper we present results from self-consistent full-potential local-orbital calculations using the FPLO-package [16, 17]. All calculations use density functional theory (DFT). *Total energies* of stacking faults are calculated within the local density approximation (LDA) (PW92 [18]). The LDA has been chosen for the total energy, because it benefits from a cancellation between the over-binding (characteristic for the LDA) and the neglected van-der-Waals interaction. By minimizing the total energy the LDA provides rather precise values for the lattice constants of hexagonal graphite (see [10] and our results below). For

the *one-electron spectra* we used the generalized gradient approximation (GGA) (PBE96 [19]), because the LDA fails to reproduce the characteristic four-leg structure of the electron pocket in hexagonal bulk graphite (see Sect. II). The GGA, on the other hand, which in many cases provides more accurate lattice constants than the LDA, fails to describe the binding between graphene layers (see also [20]). All calculations on one-electron spectra were done with the experimental C-C distance within the layers of 1.42 Å and an interlayer distance of 3.33 Å [12]. The lattice constants from total energy calculations are separately discussed in the text.

Band weights $W_\nu(\mathbf{k}, n) = |\langle \nu | \mathbf{k}, n \rangle|^2$ represent the size of the contribution of local orbital $|\nu\rangle$ to the Bloch wave function $|\mathbf{k}, n\rangle$. The sum of all orbital weights is normalized to unity

$$\sum_{\nu} W_\nu(\mathbf{k}, n) = 1. \quad (1)$$

In the plots with band weights, the local orbitals $|\nu\rangle$ are represented by the form and color of symbols at the energy bands, and the band weights by the size of the symbols. Because for *bulk states* the band weights converge to constants $W_\nu^{bulk}(\mathbf{k}, n)$ away from surfaces/interfaces, it follows from the sum rule (1) that W_ν^{bulk} scales like $1/N_{\parallel}N_{\perp}$, where N_{\parallel} and N_{\perp} are the number of atoms in a layer and the number of layers in a slab, respectively. For *surface / interface states* the band weights converge to zero, and consequently the band weights scale like $1/N_{\parallel}$. This means that for bulk states the band weights at each site are decreasing with growing slab thickness, whereas for surface / interface states they become independent of the thickness. For thick slabs the largest band weights for surface / interface states (in the vicinity of the surface / interface) are therefore much larger than for bulk states.

The local density of states (LDOS) is defined as

$$D_\nu(E) = 2 \sum_{\mathbf{k}, n} W_\nu(\mathbf{k}, n) \delta(E - \varepsilon_n(\mathbf{k})) \quad (2)$$

and integrates to 2 electrons. All \mathbf{k} space integrations were done with the tetrahedron method [21, 22].

II. BULK GRAPHITE

A. Band structure

Despite the fact that hexagonal bulk graphite has already been the subject of numerous works (see e.g. reviews on older work [8, 23], and the more recent self-consistent calculations using LDA, GGA, and GW [9, 10, 20, 24]), we have to say a few words about it. This is because we want to demonstrate the results of our approach in the bulk limit, and to introduce the projected bulk band structure (PBBS) of hexagonal graphite. If not otherwise indicated, the \mathbf{k} -mesh for the self-consistent calculation on bulk hexagonal graphite

comprises 500x500x100 inequivalent points distributed equidistantly over the Brillouin zone (BZ).

Fig. 1 gives an overview over the bulk band structure in GGA showing that ε_F lies in a gap of the σ -bands of width ≈ 11 eV and that all the Fermi surface physics comes from p_z bands. Perpendicular to the layers, bulk hexagonal graphite consists of linear chains of atoms with overlapping p_z orbitals and single atoms (monomers) with dangling p_z bonds (see Fig. 2). Fig. 3 and Fig. 4 show that it is mainly the single atoms which carry the states around ε_F . In particular, the states of the degenerate very flat band with 20 meV dispersion between K and H carry only weights from the single atoms (Fig. 3). The other bands with about 1 eV dispersion between K and H carry only weights from the chain atoms. The small dispersion of the single-atom bands is due to their dangling bonds. The two peaks in the LDOS near ε_F in Fig. 4 are produced by the two extrema seen in the left panel of Fig.3, which refers to the central plane of the BZ at $k_z=0$.

Our Fermi surface (FS) in GGA shows the generally accepted four-leg topology of the *majority electron- and hole pockets*, which are located correctly within the BZ. The only qualitative difference in our LDA results (not shown) is that the maximum of the downward bent parabola in the left panel of Fig. 3 lies slightly (by 0.5 meV) above ε_F . This tiny shift has the consequence that the electron pocket decomposes into 4 pieces, just as reported in the LDA approach by Ref. [24]. Therefore, we used the GGA for the calculation of all one-particle spectra.

In the literature there has been a lengthy debate about the number and location of tiny *minority pockets*, which depend sensitively on the sign and size of the small overlap integrals (mainly γ_6) of the Slonzewski-Weiss-McClure (SWM) model [25, 26] (see review [8]) and, from the experimental side, on the characteristics of the samples. Even recently appeared papers on the interpretation of the de Haas - van Alphen data [27, 28] indicating that the matter is still in discussion. With our DFT calculations we did not find any minority pockets, which seems to be a general trait of self-consistent DFT and GW calculations [9, 24]. This problem can be fixed by introducing artificial doping [9], but we did not take any measures in order to make the FS agree with the SWM model in the issue of the tiny minority pockets.

B. Projected bulk band structure

The PBBS is a useful tool to separate surface- or interface bands of thick slabs from bulk bands without investigating all slab wave-functions in detail, but just by locating their energy relative to the PBBS. The PBBS is defined as follows: Assume that the slabs to be investigated extend in the $x - y$ plane and calculate the bulk band structure (BBS) $\varepsilon_n^{\text{bulk}}(k_x, k_y, k_z)$ with macroscopic periodic boundary condition in all 3 dimensions. Then plot $\varepsilon_n^{\text{bulk}}(k_x, k_y)$ for all n and for a quasi-continuous set of k_z values:

$$\varepsilon_n^{\text{PBBS}}(k_x, k_y) \stackrel{\text{def}}{=} \{ \varepsilon_n^{\text{bulk}}(k_x, k_y, k_z) |_{k_z} \} \quad (3)$$

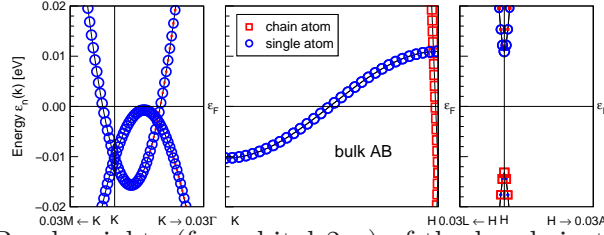


FIG. 3. (color online) Band weights (for orbital $2p_z$) of the bands in the vicinity of the line K-H at the two Wyckoff positions (single and chain atom) in hexagonal bulk graphite. The scale of the lines on M-K- Γ and L-H-A is the same, but differs from the scale of K-H. Only those 3% of the lines M-K, K- Γ , L-H, and H-A are shown, which lie closest to the points K or H. As to the notation of the end points: the point $K \rightarrow 0.03 M$ lies on the line K-M, shifted by 3% from point K toward point M, etc.

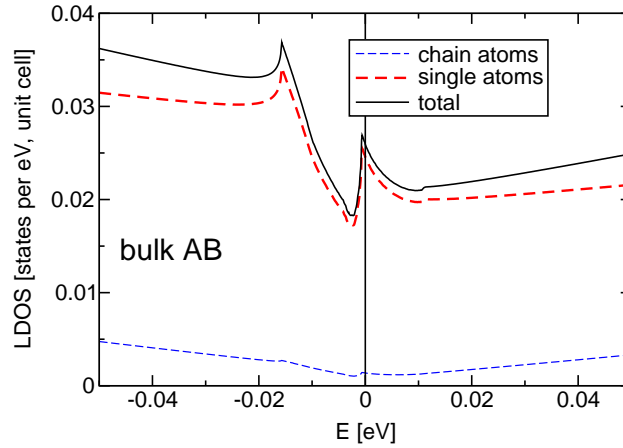


FIG. 4. (color online) LDOS of hexagonal bulk graphite (projection on all orbitals per site). The Fermi level in all LDOS plots is at zero energy. The LDOS has been calculated with a special tetrahedron mesh located in a restricted part of the BZ around the line K-H including $150 \times 150 \times 150$ points.

The resulting distribution will show broad quasi-continuous bands and gaps (see Fig. 5 in case of hexagonal graphite for 11 k_z values).

For bands in slabs in the limit of infinite thickness (but *without* periodic macroscopic boundary conditions in z -direction) the following statements hold [29]:

- (i) Slab bands which lie in gaps of the PBBS are surface- or interface bands *localized* in z direction toward the interior of the slab.
- (ii) Slab bands which lie in (quasi-continuous) bands of the PBBS agree exactly in energy with the corresponding band of the BBS, and their density agrees in the interior of the slab with that of the bulk bands.
- (iii) Slab bands within a gap, but close to the edge of a (quasi-continuous) band of the PBBS, have weak localization (large decay length).

Of course, numerical slab calculations are done on slabs of finite thickness. In case of any reasonable doubt concerning the character of the band, if slab bands are very close to band edges of the PBBS, one can obtain certainty only by analyzing the spatial localization of the slab wave-function, e.g., by calculating the band weights.

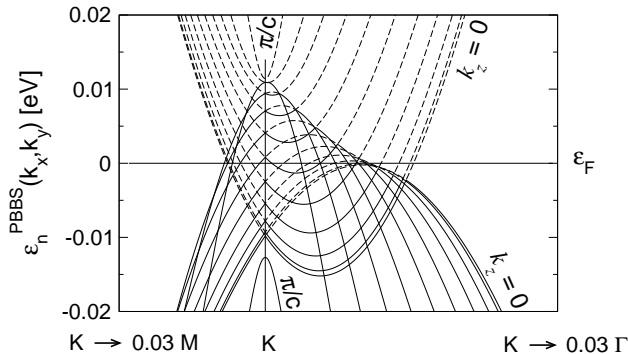


FIG. 5. Bulk band structure of (AB) graphite projected onto a plane parallel to the layers for 11 equidistant k_z values. Only 3 % of the lines M-K and K- Γ in the \mathbf{k}_{\parallel} -space, centered around symmetry point K, are shown. Full and dashed lines denote the valence and conduction band, respectively.

C. Total energy

In order to check the possibility to use the LDA for total energy calculations of graphitic systems we first calculated the optimized lattice constants of bulk (AB) and (ABC) structures and compared their total energies. Despite the missing van-der-Waals correction, we observe in Table I still some overbinding characteristic of the LDA, but all in all, the LDA does well for the lattice constants. From Table II we can learn that the total energies of hexagonal (AB) and rhombohedral (ABC) graphite are very close in energy, whereas hypothetical hexagonal (A) stacking is well above. The latter result justifies the neglect of stacking orders with two identical neighboring layers for realistic systems. However, (ABC) has a lower energy than (AB) despite the fact, that natural graphite is predominantly (AB) ordered. Because the energy difference is less than one meV, we not only did these total energy calculations with an increased numerical precision of the overlap integrals [30] and checked the convergence in the number of \mathbf{k} points carefully (see below), but we tried also the GGA, the LDA with Perdew-Zunger XC, and we added an extra shell of orbitals to the default basis set. None of these modifications reversed the ordering of the energies or changed essentially the energy difference. Consequently, either the correct energetic order of (AB) and (ABC) graphite is beyond the possibilities of the LDA and the GGA, or, the

system		exp.	opt.
(AB)	a	2.4595	2.450
	c_{nn}	3.33	3.306
(ABC)	a		2.450
	c_{nn}		3.305

TABLE I. Experimental and LDA-optimized lattice constants of bulk (AB) and (ABC) graphite in Å. The in-plane lattice constant is denoted a and c_{nn} is the distance between two layers. The \mathbf{k} mesh for the optimization comprised 50 points in each dimension for both structures.

system	exp.	opt.
(AB)	0	-1.1
(ABC)	-0.2	-1.2
(A)	+15.7	

TABLE II. Total energies per atom in meV for the experimental and the optimized lattice constants (from Table I) for bulk (AB), (ABC) and (A) stackings in LDA. The reference energy is the energy for (AB) graphite from the experimental lattice constant.

electronic part of the total energy in (ABC) is really lower than in (AB), but the here disregarded *phononic part* plays a decisive role for the ground state. In principle, there is also the possibility that the larger probability for (AB) ordering in natural graphite is due to special crystal growing conditions (temperature, pressure, etc.) and that (AB) graphite is a meta-stable state under ambient conditions like diamond.

The authors of Ref. [10] obtained for (AB) a total energy, which lies 0.1 meV *below* the total energy of (ABC) graphite. They however used the Monkhorst-Pack procedure with 28 special points (in the irreducible BZ) amounting to some hundred points in the full BZ. Fig. 6 shows, that up to some 10 000 (equidistant) points for the tetrahedron method the total energies for both structures oscillate wildly making a save calculation of such a small energy difference impossible. It is clear that the Monkhorst-Pack procedure has another convergence behavior than the tetrahedron method, but on the other hand it is not clear at all, whether it is suited for high precision demands on semi-metals like (AB) graphite, because it is tailored for semi-conductors and insulators.

D. Estimate of the van-der-Waals correction

In order to find out, if the consideration of the van-der-Waals interaction can clarify the situation, we estimated its impact on the total energies using the semi-empirical approach

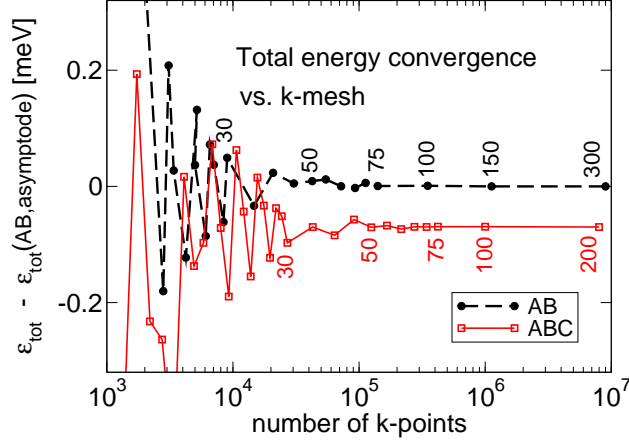


FIG. 6. (color online) Convergence of the total energy in LDA of (AB) and (ABC) graphite versus the total number of \mathbf{k} points in the BZ on a logarithmic scale. For both structures the optimized lattice constants as given in Table I were used. The reference energy is the asymptotic value for (AB) graphite. The numbers next to some points for (ABC) graphite indicate the number $N_1 = N_2 = N_3$ of k-points in each direction of the rhombohedral BZ. For hexagonal (AB) graphite the number $N_1 = N_2$ of k-points in the plane parallel to the layers is given, whereby the number N_3 of k-points perpendicular to the layers has been chosen the closest integer of $1/3$ of this number. The step width for N_1 is 1 for $N_1 \leq 30$ and 5 for $30 \leq N_1 \leq 75$.

by Grimme *et al.* [31] in the version DFT-D2 [32]:

$$E_D = s_6 \sum_R f(R) \frac{C_6}{R^6} \quad (4)$$

with the damping function

$$f(R) = [1 + e^{-d(R/R_0-1)}]^{-1} \quad (5)$$

The sum runs over inter-atomic distances R (calculated from experimental lattice constants of (AB) graphite), the scaling factor is $s_6 = 1.1$, $d = 20$, and for carbon the dispersion coefficient and the van-der-Waals radius amount to $C_6 = 1.75 \text{ J nm}^6 \text{ mol}^{-1} = 18.1 \text{ eV \AA}^6$ and $R_0 = 1.452 \text{ \AA}$, respectively.

We took into account only inter-layer contributions, because the intra-layer contributions are independent of the stacking sequence. It turns out, that the Grimme correction per atom to the total energy of bulk (AB) and (ABC) amounts to -210.4284 and -210.4289 meV, respectively, providing a difference of $0.5 \mu\text{eV}$ in favor of (ABC) graphite. One reason for this minute difference is the fact that the interaction energy of two layers is independent of their type (provided they are not identical) and therefore only next-nearest (and beyond) layer interactions contribute to the energy difference between two stacking orders. Second, even if there is a difference, it is minute. There are only two values for the interaction between two arbitrary layers depending on whether they are identical (say A-A) or different

(say A-B). The interaction energy of the two atoms in layer A with a full layer A for next nearest neighbor layers is 12.161923 meV versus 12.161918 meV for A-B. Consequently, the van-der-Waals correction at least in the semi-empirical Grimme form can be safely neglected for the energy difference between stacking orders.

III. SURFACE OF GRAPHITE

Graphitic slabs are numerically demanding in three ways:

- (i) Because graphite is a semi-metal with a tiny Fermi surface around the K-point, one needs a large number of \mathbf{k} points in order to get the essential features of the FS well resolved and an accurate position of the Fermi level. For the self-consistent calculation we used a \mathbf{k} grid of 240x240x1 inequivalent points. For the LDOS near ε_F we chose a special grid of points, which is restricted to the vicinity of the K-point and comprises 150x150x1 points.
- (ii) Due to the small density of states near ε_F the screening of perturbations may extend over long distances. Thus, the slabs used in the numerical calculation have to be chosen rather thick, if separated interfaces or surfaces shall be described. For slabs, which are thick enough, extra layers within the given building scheme should not have an impact on the physical results.
- (iii) Thick slabs with low symmetry tend to have problems in converging to self-consistency. Therefore, it is vital to use the highest possible symmetry. This can be achieved by choosing an appropriate number of layers (see Sect. IV-VI).

A. Band structure of (AB) slabs

We consider a clean surface, which can be studied by means of a thick slab. Fig. 7 shows band weights in $(AB)_{16}$ for a few prominent local orbitals and Fig. 8 presents the corresponding LDOS. For a visualization of the atomic positions in the slab see the right part of Fig. 2. As to p_z -bonding, which is crucial for the electronic structure around the Fermi energy, we again distinguish single atoms (monomers) and chains, which are now finite.

First, in Fig. 7 we observe no low-energy surface bands separated from the bulk continuum. This refers to higher energies in the range of the π and σ bands on the symmetry lines as well (not shown in our figures) in accordance with Ref. [20]. In contrast, the LDOS in Fig. 8 reveals that around ε_F there is a *depletion* of electrons in the surface layer rather than an accumulation (which would be expected for surface states). It should be expected that the bulk LDOS in Fig. 8 converges to the bulk curves shown in Fig. 4 in the limit of infinite thickness of the slab. This is already suggested by Fig. 8, except for the peak just above the Fermi energy $\varepsilon_F = 0$, which is decomposed into a bunch of single peaks. Closer inspection of the band structure in the energy region around ε_F (not shown) reveals that

these peaks are mainly due to van-Hove singularities caused by avoided crossing of bands, which gradually disappear if the number of bands goes to infinity.

Second, Fig. 8 also shows that the bands near ε_F are mainly localized at the single atoms. Considering the results of the previous paragraph, the latter conclusion is not surprising because the band structure of a thick slab must be similar to the PBBS, if no surface bands exist. Fig. 8 shows that the LDOS around ε_F at single atoms in the bulk is one order of magnitude larger than at chain atoms in agreement with the bulk calculation in Fig. 4.

In terms of the local conductivity these two points lead to the conclusion that one should expect a depletion of conductivity in the surface layer and current flow mainly through hopping between single atoms. The strong asymmetry regarding the two atomic positions at the surface in the LDOS near the Fermi energy explains also the strong asymmetry of the two sites in STM images [33].

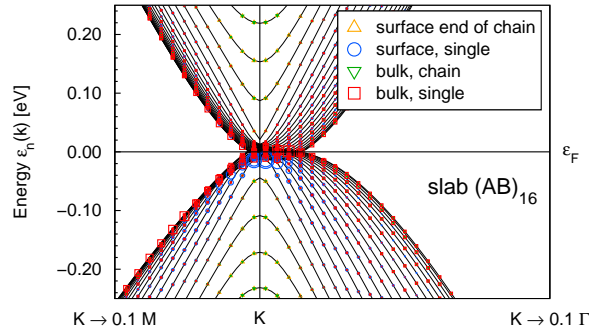


FIG. 7. (color online) Band weights of the local orbital $2p_z$ located at the surface and in the middle (denoted 'bulk') of the slab $(AB)_{16}$.

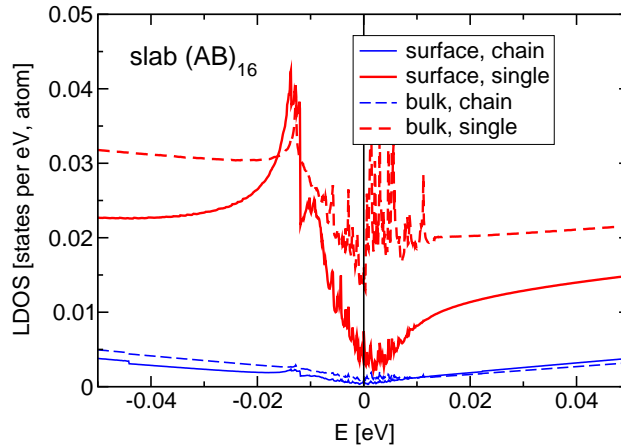


FIG. 8. (color online) Surface versus bulk LDOS (sum of all orbitals per lattice site) in the $(AB)_{16}$ slab.

B. Surface energy

We use the standard definition of the surface energy per surface atom

$$e_s = \frac{1}{4}(E_{sc} - N_{at} \cdot e_b) \quad (6)$$

where E_{sc} is the total energy of the super-cell with N_{at} atoms and e_b is the total energy per atom for the bulk. Because each super-cell has two surfaces and two surface atoms on either surface, we introduced the factor $1/4$ in the definition. In principle the result of Eq. (6) might depend on the thickness of the layer, but has to converge in the limit of infinite thickness, provided, E_{sc} is calculated in the interior of the slab with the same precision as e_b [34]. We met this demand by using the same program with the same parameters and the same \mathbf{k} grid in the plane parallel to the layers (120x120x50 and 120x120x1 for the bulk and the slabs, respectively). Our results shown in Fig. 9 are not yet fully converged, but a tendency toward convergence is obvious. In order to obtain an approximate asymptotic value e_∞ , we adapted the three parameters of the ansatz $e_s(n) = e_\infty + a \exp(-b n)$ to the three calculated values at $n = 4, 12$, and 20 , where our slab $(AB)_n$ consists of n formula units. We found $e_\infty = 8.12$ meV, $a = 0.305$ meV, and $b = 0.165$. The corresponding curve is plotted in Fig. 9. Experimental values for (AB) graphite lie in the wide range of (2.83 - 18.9) meV/surface atom (see Table 5 in [20]) and the result for $n = 12$ using Eq. (6) and the VASP code is 7.92 meV/surface atom [20].

Although we cannot reach full numerical convergence of e_s with layer thickness, it is worthwhile to compare surface energies for the surfaces of (AB) and (ABC) graphite for the same number of layers. Calculations for slabs with super-cells $(AB)_6$ and $(ABC)_4$ (both have 12 layers) provide $e_s = 8.23$ meV and $e_s = 8.38$ meV, respectively. From a local point of view the smallness of the difference between the two systems seems understandable, because both surfaces differ only in the third layer from the surface inward. On the other hand, both systems differ qualitatively in their electronic structure. Whereas (ABC) graphite has around ε_F topologically protected surface states and a Dirac-like band structure in the bulk limit [15], (AB) graphite is a semi-metal with a small Fermi surface and without surface states in the whole region of π and σ bands.

IV. STACKING FAULTS

For the calculation of one-particle energies and derived properties we used a periodic arrangement of slabs which are surrounded by vacuum and which have **one** stacking fault in the middle. The alternative model is a periodic arrangement (without vacuum) with **two** stacking faults per unit cell in order to obtain periodicity, which has been adopted for total energies (see Introduction). We want to stress that for the size of slabs presented here there is no remarkable difference between both models in the local properties like LDOS and band

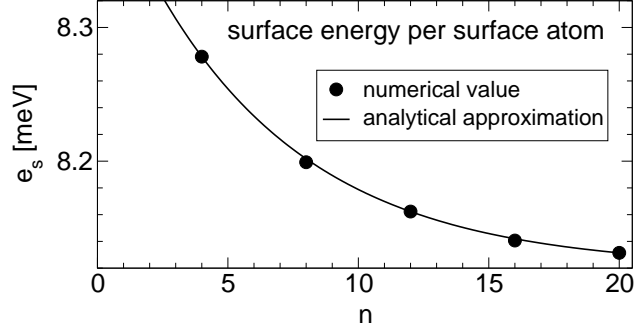


FIG. 9. Convergence of the surface energy per surface atom versus the number of unit cells in slabs $(AB)_n$.

weights for atoms close to the stacking faults. All self-consistent calculations on slabs have been done with a \mathbf{k} mesh of $120 \times 120 \times 1$ points equal-distantly distributed over the BZ. Test calculations with $240 \times 240 \times 1$ points did not show any visible changes. For the calculations on periodically repeated super-cells we used a grid of $150 \times 150 \times 10$ points.

Fig. 10 gives the essential structural information on the two possible types of stacking faults in hexagonal graphite, denoted α and β . The number of layers has been chosen in such a way that the highest possible symmetry (and therefore precision for given computational resources) could be achieved. Whereas bulk hexagonal (AB) graphite has two Wyckoff positions, namely single atoms (monomers) and atoms on infinite chains with saturated p_z orbitals, the chains are terminated at the surface and the interfaces ending with dangling bonds. The crucial difference as to local bonding between type α and β interfaces is the following: Type α has a dimer bridging the stacking fault, with a related small interlayer overlap γ_1 and indirect overlap between the chains on both sides of the fault via the dimer. In type β , the dangling bonds of two adjacent chains overlap laterally with the large overlap integral γ_0 .

A. Band structure

Figs. 11 and 12 show the energy bands with the most prominent band weights for α and β interfaces around the K-point. We observe that for both interfaces there is an occupied and an empty interface band close to the bulk continuum, except in the very vicinity of the K point. In either case, the interface bands are located mostly at the monomers closest to the interface (atom # 6 in Fig. 10), i.e., they are formed by the dangling p_z -bonds of these monomers. The band weights of the monomers further away from the interface (e.g. # 4 in Fig. 10) in the interface bands are already small and would not be visible in these figures. This means that the amplitude of the interface bands converges rapidly to zero toward the bulk. Exceptions are the interface bands on the line K- Γ in type β . Their distance from the bulk continuum is smaller and their localisation is weaker than for the other interface

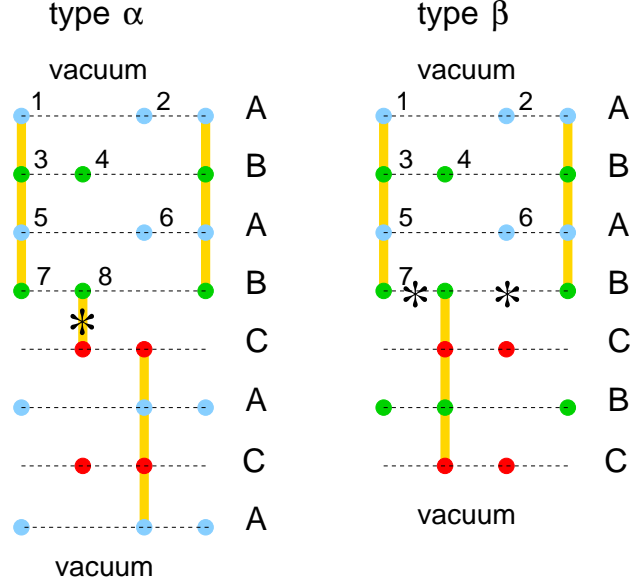


FIG. 10. (color online) Examples for the two types of stacking faults in highly symmetric slabs separated by vacuum slabs. Left panel: type α : $(AB)_n(CA)_n$ and right panel: type β : $(AB)_n(CB)_{n-1}C$, both for $n = 2$. (The numerical calculations presented below were done for $n = 8$.) The yellow perpendicular bars indicate saturated p_z bonds and the stars mark inversion centers. Both types of slabs have the symmetry $P\bar{3}m1$.

bands. Therefore, the existence of an interface state in this \mathbf{k} region in the limit of infinite thickness is not absolutely certain.

Comparison of our results for type β with the model calculations in Refs. [6] and [7] shows little similarity apart from the mere existence of interface states. The main difference is that in our calculation the interface states vanish in the very vicinity of the K-point due to the presence of bulk states. The low-energy dispersion of these bulk states is not correctly described by simple models with only two overlap parameters.

Fig. 13 shows another interesting feature. There are occupied and empty bands localized at the dimers of interface α , which are split by approximately 0.8 eV at the K-point (see lower panel). This splitting agrees with the value, which is expected for the splitting of the p_z levels in an *isolated dimer* $E_{\pm} = E_0 \pm \sqrt{|\gamma_1|^2}$ due to an empirical overlap integral with the generally accepted value $\gamma_1 \approx 0.4$ eV. Near the K-point, these dimer bands are not strictly localized interface bands, but resonances with a large amplitude near the interface, because they are submerged into the the continuum of bulk states. The upper panel shows, that along the line from K toward M not only the dimer atoms get involved in the interface bands, but also the atoms at the end of the chains. Therefore, away from the K-point and at energies of the eV-range, the interface bands are no longer localized solely at monomers. Inspection of the other parts of the 2D BZ (which are not shown in the figures) shows that *on the symmetry lines* interface states are only found on the line K-M and on small parts of

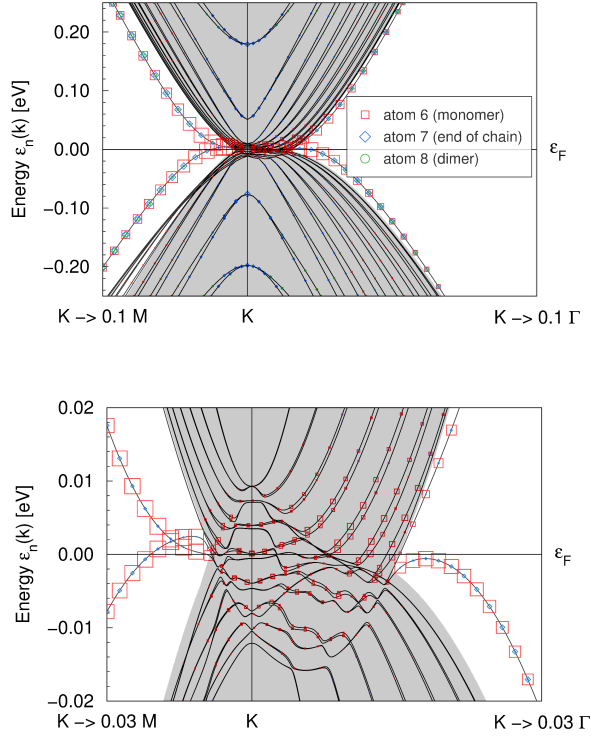


FIG. 11. (color online) Band weights of the orbital $2p_z$ close to a stacking fault of type α for $(AB)_8(CA)_8$ with two energy scales. The atom numbers 6 to 8 refer to atoms in the two layers next to the fault, as defined in Fig. 10.

the lines M- Γ and K- Γ . In other words, they are virtually restricted to the symmetry lines shown in the upper panel of Fig. 13.

Fig. 14 presents the LDOS near both types of interfaces and near the surfaces compared with the bulk DOS. In either case the interface bands produce strong low-energy peaks in the LDOS for the monomers closest to the interface, but in type α the peak is most pronounced.

Fig. 15 presents the LDOS of slabs with interface α for different thickness of the slab. One notes that even a slab with one graphite unit cell on both sides of the stacking fault ($n=1$) shows a pronounced peak and is thus a suited model for studying the interface bands, although the specifics of the low-energy electronic structure depend on the slab thickness, which is seen in the form of the LDOS.

B. Formation energy of stacking faults

The total energies of systems with stacking faults were calculated using super-cells without surfaces (see Introduction). For stacking fault α and β the unit cells $B(AB)_n(CA)_nC$

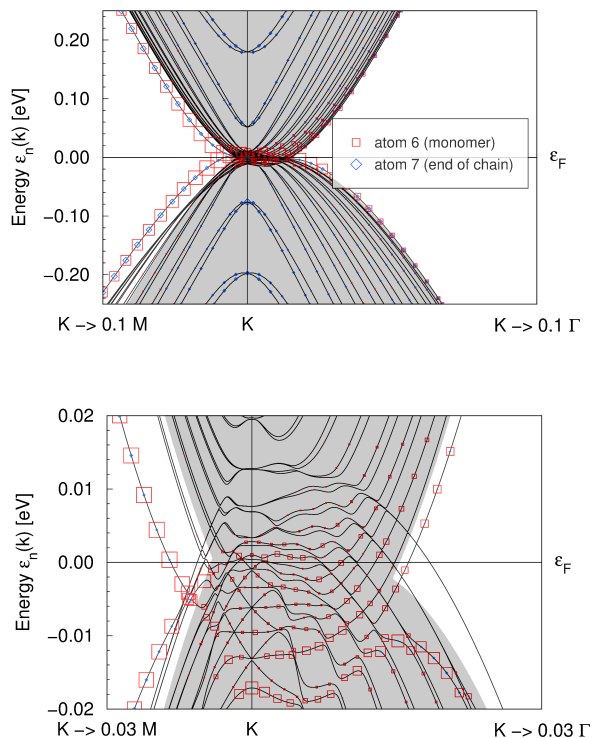


FIG. 12. (color online) Band weights of the orbital $2p_z$ close to a stacking fault of type β for $(AB)_8(CB)_7C$. Further details as in Fig. 11.

and $(BA)_n(BC)_n$, respectively, with $n = 4$ and 8 were used (see Fig. 16). They differ slightly from the cell in the geometry with surfaces, because this allows to retain the high symmetry of bulk AB graphite (group $P6_3/mmc$). The difference concerns only the exact number of layers per block, which should be irrelevant for the electronic structure around the stacking faults, if the blocks are thick enough.

The interface contribution to the total energy per interface atom is defined in analogy to the surface energy Eq. (6) as

$$e_{if} = \frac{1}{4}(E_{sc} - N_{at} \cdot e_b) \quad (7)$$

The factor $1/4$ comes from the fact that we have two stacking faults per unit cell and two atoms in the interface layer. The interface energy e_{if} shown in Table III shows that the total energy of a slab with interface α lies only slightly above pure bulk, whereas the extra energy of interface β is somewhat larger. The values also depend on whether we use the experimental or the theoretical lattice constants. We further observe, that in the range of 18 to 34 layers the interface energy still depends slightly on the width of the bulk blocks, which is in agreement with the convergence behavior of the surface energy discussed in Sect. III B.

The energetic advantage of stacking fault α versus β could be understood with the ex-

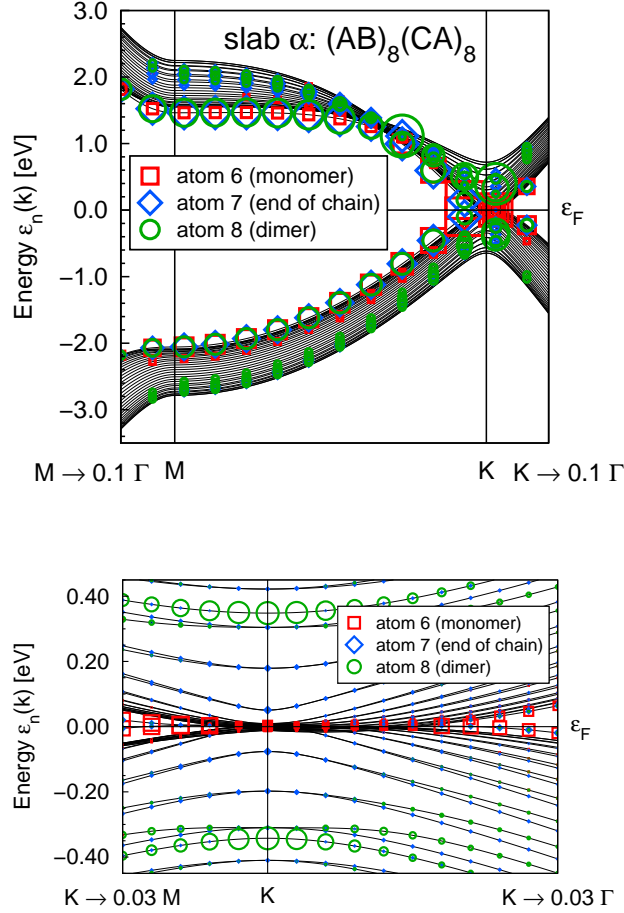


FIG. 13. (color online) Band weights of the orbital $2p_z$ close to a stacking fault of type α for $(AB)_8(CA)_8$. Upper panel: line K-M and parts of the adjacent symmetry lines, lower panel: blow up of the lines K-M and K- Γ around the point K. For a better overview, in the upper panel all symbols are omitted, which are smaller than 50% of the maximum size. The big green circle in the conduction bands just right of the vertex of bands is not a numerical fluctuation, but an indication for a genuine strong variation of the band weights in this region of the \mathbf{k} space.

istence of the (occupied) dimer band in the former, which lowers the sum of one-particle energies as an important part of the total energy. If the electronic part of the total energy is a measure for realization of the structure, this result would make interface α more likely to occur in real crystals than interface β . Consider, however, that the energy differences of the electronic part are of order 10^{-5} eV, and that the effects discussed in Sect. II C can have a strong impact as well.

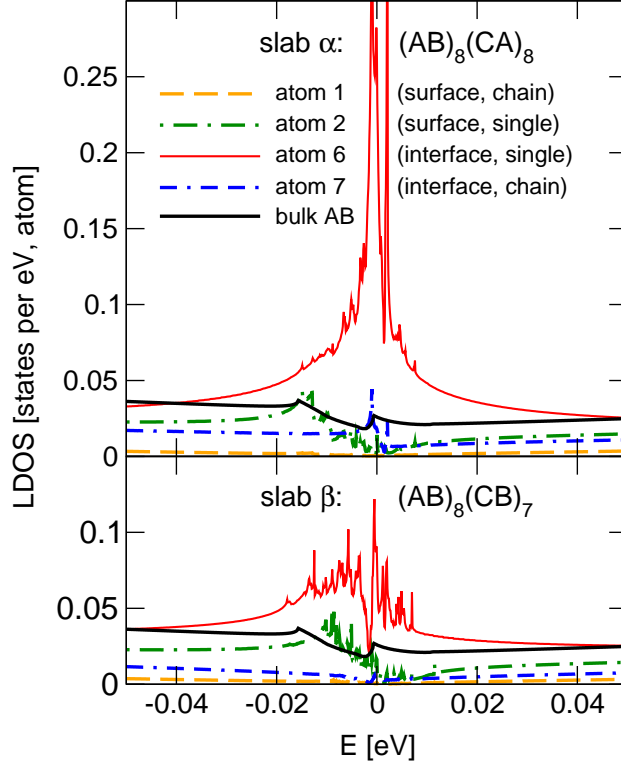


FIG. 14. (color online) LDOS (sum of all orbitals per site) at atoms near the surface and near the interface in a slab of type α for $(AB)_8(CA)_8$ (upper panel) and a slab of type β for $(AB)_8(CB)_7C$ (lower panel) compared with the bulk DOS. For the LDOS a special mesh of $150 \times 150 \times 1$ points located in a restricted area around the K point was used.

V. DISPLACED SURFACE LAYER

We have shown above that there are no surface bands in hexagonal graphite, but stacking faults can induce interface bands. The next issue is, if only *one* displaced surface layer with the geometry shown in Fig. 17 can do this job. The resulting band structure with band weights in Fig. 18 shows that at least on the line K - M there is a surface band which is mostly localized at the monomers 2 and 6 defined in Fig. 17. On the line K - Γ there are surface resonances with increased weights toward the surface, but no real surface bands. Note that the structure has dimers at the surface which produce localized dimer bands (not shown) split by approximately 0.8 eV similar to the dimers near stacking faults. These dimer bands look very similar to those shown in the lower panel of Fig. 13 for a slab with stacking fault α , but each dimer band is almost doubly degenerate with a slight splitting. This is due to the existence of two dimers in the unit cell of the slab (one on either surface) with a small interaction through the slab.

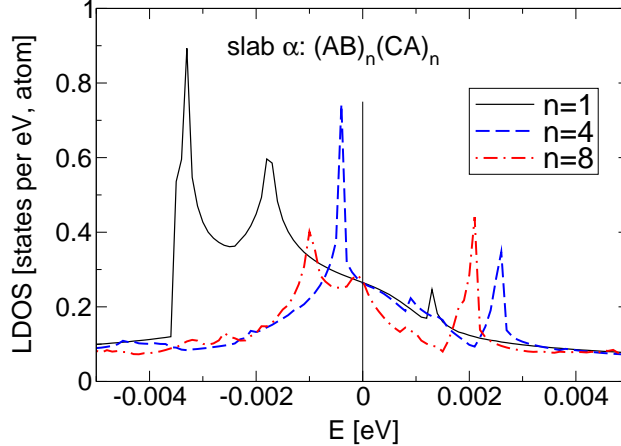


FIG. 15. (color online) LDOS (sum of all orbitals per site) at the atoms # 6 (monomer closest to the stacking fault) in slabs $(AB)_n(CA)_n$ for several values of n . (Observe the zoomed scale of the E-axis compared with the other LDOS-figures.)

system	formula	e_{if}
α	$B(AB)_4(CA)_4C$	9.5 (23.4)
α	$B(AB)_8(CA)_8C$	7.9
β	$(BA)_4(BC)_4$	34.6 (43.5)
β	$(BA)_8(BC)_8$	33.5

TABLE III. Interface contribution to the total energy per interface atom, e_{if} , as defined in the text (in μeV) for hexagonal graphitic stacks in LDA. For the upper line in each block, the experimental lattice constants of (AB) graphite are used for all stacking sequences, and for the numbers in parentheses the optimized theoretical lattice constants from Table I are applied. For the matrix elements the increased precision [30] is applied throughout.

VI. SUMMARY

We investigated the electronic structure of hexagonal graphite without and with surfaces and stacking faults using self-consistent full-potential DFT calculations in the LDA and the GGA. There are two types of stacking faults (denoted by α and β) which differ in the first place by their chemical bonding of the $2p_z$ orbitals in the vicinity of the stacking fault (see Fig. 10). We find that

- *Pure surfaces* do not host any surface bands in the energy range of the π and σ bands. Because the LDOS around ε_F in the surface layer is reduced, we expect a

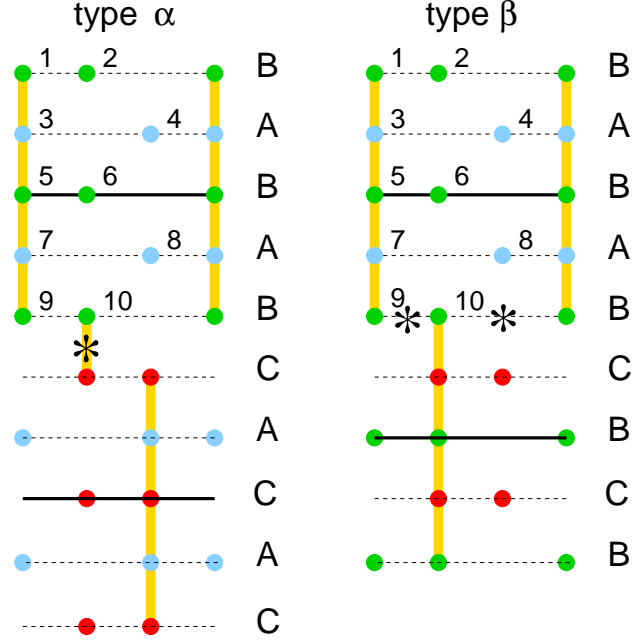


FIG. 16. Examples for the two types of stacking faults in highly symmetric super-cell geometry without surfaces. Type α : $B(AB)_n(CA)_n C$ and type β : $(BA)_n(BC)_n$, each for $n=2$. (The numerical calculations presented here have been done for $n = 4$ and 8 .) The stars denote inversion centers and the full lines mirror planes. Observe that the lowest layer in the right panel does not contribute to the formula for the unit cell because it is at the bottom of the cell and therefore equivalent to the highest, whereas all layers of the left panel are in the interior of the cell.

reduced surface conductivity compared with the bulk. Both, at the surface and in the bulk, the LDOS around ε_F is one order of magnitude larger for the single atoms than for the chain atoms. Therefore, all low-energy electronic properties (like electric conductivity, low-temperature thermal conductivity and specific heat) are governed by hopping processes between the dangling p_z -orbitals of the single atoms.

- Even displacement of *one* single atomic layer at the surface, which is the germ for producing a stacking fault in the crystal growing process, can induce surface bands.
- Both types of *stacking faults* induce interface bands around the K-point in the Brillouin zone. Correspondingly, the LDOS at the single atoms near a stacking fault is enhanced over the bulk value. In the case of type α the enhancement factor is of the order of 10. This indicates a large 2D electronic conductivity along the stacking fault.
- Stacking faults of type $(AB)_n(CA)_n$ (denoted by α) are characterized by p_z -bonded dimers, which produce a pair of dimer bands. They are split by about 0.8 eV at the K-point and could be probed by near-infrared spectroscopy. Within the LDA, their electronic part of the formation energy is smaller than for the alternative type $(AB)_n(CB)_{n-1}C$ (denoted by β).

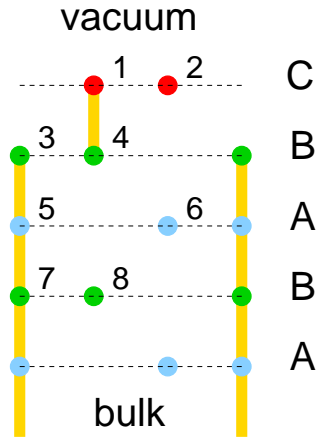


FIG. 17. (color online) Surface region of a slab $(CB)(AB)_n(AC)$ modeling hexagonal graphite with a displaced surface layer on either side.

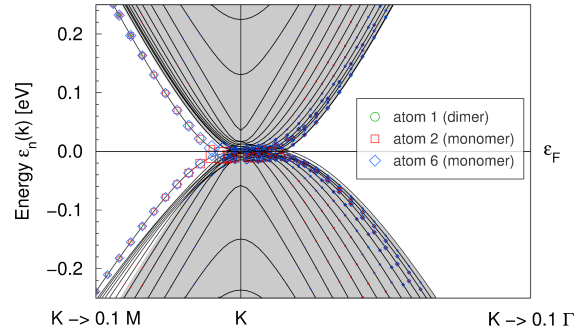


FIG. 18. (color online) Band weights of the orbital $2p_z$ near a displaced surface layer in the slab $(CB)(AB)_{10}(AC)$.

Our results indicate that it can be extremely misleading if experiments on real graphite samples (which have most likely numerous stacking faults) are compared with electronic structure calculations on ideal lattices. This applies in particular to transport measurements which are governed by the electronic structure around the Fermi energy.

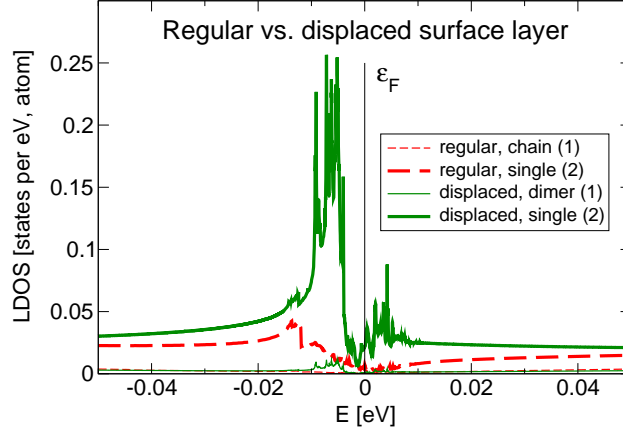


FIG. 19. (color online) LDOS (sum over all orbitals per site) at atoms on a regular and a displaced surface layer in slabs $(AB)_{16}$ and $(CB)(AB)_{10}(AC)$, respectively. The numbers in the legend refer to the atom number in Figs. 10 and 17.

ACKNOWLEDGMENTS

We are indebted to J. van den Brink, J. Venderbos, P. Esquinazi and M. Knupfer for helpful discussions. Financial support was provided by DFG Grant RI932/6-1.

-
- [1] A. H. C. Neto, F. Guinea, N. M. R. Peres, L. S. Novoselov, and A. K. Geim, *Rev. Mod. Phys.* **81**, 109 (2009).
 - [2] D. S. L. Abergel, V. Alpakov, J. Berashevich, K. Ziegler, and T. Chakraborty, *Adv. Phys.* **59**, 261 (2010).
 - [3] N. M. R. Peres, *Rev. Mod. Phys.* **82**, 2673 (2010).
 - [4] M. Goerbig, *Rev. Mod. Phys.* **83**, 1193 (2011).
 - [5] H. Kempa, P. Esquinazi, and Y. Kopelevich, *Solid State Commun.* **138**, 118 (2006).
 - [6] D. P. Arovas and F. Guinea, *Phys. Rev. B* **78**, 245 416 (2008).
 - [7] M. Koshino and E. McCann, *Phys. Rev. B* **87**, 45 420 (2013).
 - [8] N. B. Brandt, S. M. Chudinov, and Y. G. Ponomarev, *Semimetals, 1. Graphite and its Compounds* (North Holland, 1988).
 - [9] A. Grueneis, C. Attacalite, L. Wirtz, H. Shiozawa, R. Saito, T. Pichler, and A. Rubio, *Phys. Rev. B* **78**, 205 425 (2008).
 - [10] J.-C. Charlier, X. Gonze, and J.-P. Michenaud, *Carbon* **32**, 289 (1994).
 - [11] S. Latil and L. Henrard, *Phys. Rev. Lett.* **97**, 036803 (2006).
 - [12] M. Aoki and H. Amawashi, *Solid State Commun.* **142**, 123 (2007).
 - [13] H. Min, B. Sahu, S. K. Banerjee, and A. H. MacDonald, *Phys. Rev. B* **75**, 155115 (2007).
 - [14] F. Zhang, B. Sahu, H. Min, and A. H. MacDonald, *Phys. Rev. B* **82**, 35 409 (2010).

- [15] R. Xiao, F. Tasnadi, K. Koepernik, J. W. F. Venderbos, M. Richter, and M. Taut, Phys. Rev. B **84**, 165 404 (2011).
- [16] <http://www.fplo.de/>, version: 9.01-35-x86_64.
- [17] K. Koepernik and H. Eschrig, Phys. Rev. B **59**, 1743 (1999).
- [18] J. Perdew and Y. Wang, Phys. Rev. B **45**, 13 244 (1992).
- [19] J. Perdew, K. Burke, and M. Ernzerhof, Phys. Rev. Lett. **77**, 3 865 (1996).
- [20] N. Ooi, A. Rairkar, and J. B. Adams, Carbon **44**, 231 (2006).
- [21] G. Lehmann and M. Taut, phys. stat. sol. (b) **54**, 469 (1972).
- [22] G. Lehmann and M. Taut, phys. stat. sol. (b) **57**, 815 (1973).
- [23] B. T. Kelly, *Physics of Graphite* (Applied Science Publishers, 1981).
- [24] J.-C. Charlier, X. Gonze, and J.-P. Michenaud, Phys. Rev. B **43**, 4579 (1991).
- [25] J. C. Slonczewski and P. R. Weiss, Phys. Rev. **109**, 272 (1958).
- [26] J. W. McClure, Phys. Rev. **108**, 612 (1957).
- [27] I. A. Luk'yanchuk and Y. Kopelevich, Phys. Rev. Lett. **93**, 166 402 (2004).
- [28] K. Sugawara, T. Sato, S. Souma, T. Takahashi, and H. Suematsu, Phys. Rev. B **73**, 45 124 (2006).
- [29] V. Heine, Proc. Phys. Soc. **81**, 300 (1962).
- [30] Because the total energy differences between different stacking orders are exceptionally small, for the total energy calculations we used a refined real space integration mesh for the potential matrix elements. The default mesh produces noise in the 10^{-5} eV energy range, which overshadows the physical energies in this case. We increased the number of radial mesh points to 200 and used the densest implemented angular mesh with 602 points on the unit sphere for each radial shell.
- [31] S. Grimme, Comp. Mol. Sci. **1**, 211 (2011).
- [32] S. Grimme, J. Comput. Chem. **27**, 1 787 (2006).
- [33] D. Tomanek, S. G. Louie, H. J. Mamin, D. W. Abraham, R. E. Thomson, E. Ganz, and J. Clarke, Phys. Rev. B **35**, 7790 (1987).
- [34] J. C. Boettger, Phys. Rev. B **49**, 16 798 (1994).